Influence of unilateral low adhesion on transient wheel-rail rolling contact and wheel damages

Zhao, Xin; Huang, Shuangchao; Yin, Shan; Yang, Jizhong; Yang, Zhen; Tao, Gongquan; Wen, Zefeng

DOI
10.1016/j.wear.2023.205053

Publication date
2023

Document Version
Final published version

Published in
Wear

Citation (APA)
Zhao, X., Huang, S., Yin, S., Yang, J., Yang, Z., Tao, G., & Wen, Z. (2023). Influence of unilateral low adhesion on transient wheel-rail rolling contact and wheel damages. *Wear*, *530-531*, Article 205053. https://doi.org/10.1016/j.wear.2023.205053

Wear 530–531 (2023) 205053

Contents lists available at ScienceDirect

Wear

journal homepage: www.elsevier.com/locate/wear

Influence of unilateral low adhesion on transient wheel-rail rolling contact and wheel damages

Xin Zhao [a,*], Shuangchao Huang [a], Shan Yin [a], Jizhong Yang [b], Zhen Yang [c], Gongquan Tao [a], Zefeng Wen [a]

[a] State Key Laboratory of Traction Power, Southwest Jiaotong University, Chengdu, 610031, China
[b] China Railway Eryuan Engineering Group CO., LTD., Chengdu, China
[c] Section of Railway Engineering, Delft University of Technology, Delft, the Netherlands

ARTICLE INFO

Keywords:
High-speed
Wheel-rail rolling contact
Low adhesion
Vibrations
Irregular wear
Explicit FE method

ABSTRACT

A time-domain finite element model is developed to study the transient rolling contact of a driving wheelset over a curved track with Low Adhesion Zones (LAZs) shorter than 1.0 m. LAZs on one rail, i.e., unilateral LAZs occurring more likely, is treated for a speed up to 500 km/h. Structural vibrations of wheelset are analyzed to explain the transient contact forces, creepages and the resulting irregular wear. LAZs on high rails are found more detrimental than those on low rails. The results explain the occurrence of flats and rolling contact fatigue in bad weather, although significant wheel idling is absent.

1. Introduction

Wheel-rail adhesion is the physical basis of train acceleration and deceleration, thus, is a key problem that has to be treated in railway engineering. Low adhesion, as one of the oldest problems in railway, occurs when required traction or braking efforts are larger than the available adhesion, typically when contaminants such as precipitation, leaking oil and fallen leaves are present in the wheel-rail interface [1–3]. The direct consequence of low adhesion is wheel slip on rail with large creepages, because of which a train is out of control to a certain extent, further leading to problems such as delays in the train service, signals passed at danger, station platform overruns, and even collisions [4,5]. To prevent excessive wheel slide, in the worst case wheel idling in traction and locking in braking, and make full use of available adhesion, anti-slip control has usually been implemented in both Traction Control (TC) and Wheel Slide Protection (WSP, for braking) systems on modern trains together with adhesion enhancement measures such as sanding and friction modifiers [1,3,6,7].

On Jan. 4, 2018, in a depot of high-speed electrical multiple units (EMU) located in central China, severe rolling contact fatigue (RCF) was found on 11 EMU trains after one-day running in heavy snow at 300 km/h max. Fig. 1(a) shows a typical tread taken in the depot, for which all damaged wheels were turned on lathes immediately. Preliminary investigations showed that most severely damaged wheels were of motor cars and anti-slip control had been triggered on most damaged wheels. In the absence of precipitation, however, no similar problems have been observed. Further considering the general understanding that snow and the melting water may lead to low adhesion, and water trapped in cracks can accelerate the crack propagation through the mechanisms of pressurization at crack tips and lubrication between crack faces, the root cause of the RCF damage, to the authors' best knowledge, should be low adhesion and the resulting large slip occurring under traction in that day.

It should be noted that the anti-slip control operations were not triggered continuously on the fatigued wheels, and even absent on a few, although heavy snow was everywhere. The reason of such a phenomenon may be two-fold: 1) only Low Adhesion Zones (LAZs) long enough can lead to creepages larger than thresholds of anti-slip control and trigger its operation; 2) creepages larger than the thresholds but lasting insufficiently long also fail to trigger the operation due to limited sampling frequencies or the design principle of an anti-slip control system. Short LAZs may not trigger anti-slip control, but the resulting adhesion saturation and relatively large creepages can still result in RCF after a running distance of sufficient length.

Long flats occurring on one wheel of a wheelset are another type of damage observed occasionally on high-speed EMU wheels, as shown in Fig. 1(b). Their one-side occurrence is not in line with the traditional understanding that flats occur in pair on both wheels. Since such a

* Corresponding author.
E-mail address: xinzhao@swjtu.edu.cn (X. Zhao).

https://doi.org/10.1016/j.wear.2023.205053
Received 26 February 2023; Received in revised form 19 May 2023; Accepted 11 July 2023
Available online 13 July 2023

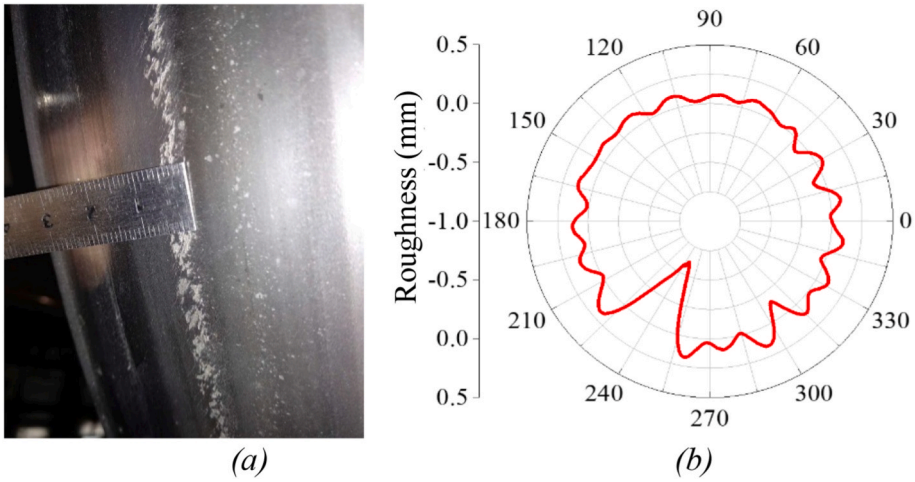

Fig. 1. Damages found on high-speed EMU wheels: (a) RCF on a wheel after running in a heavy snow day at 300 km/h max. (b) A long flat on a wheel running 200 km/h max (about 27 cm long).

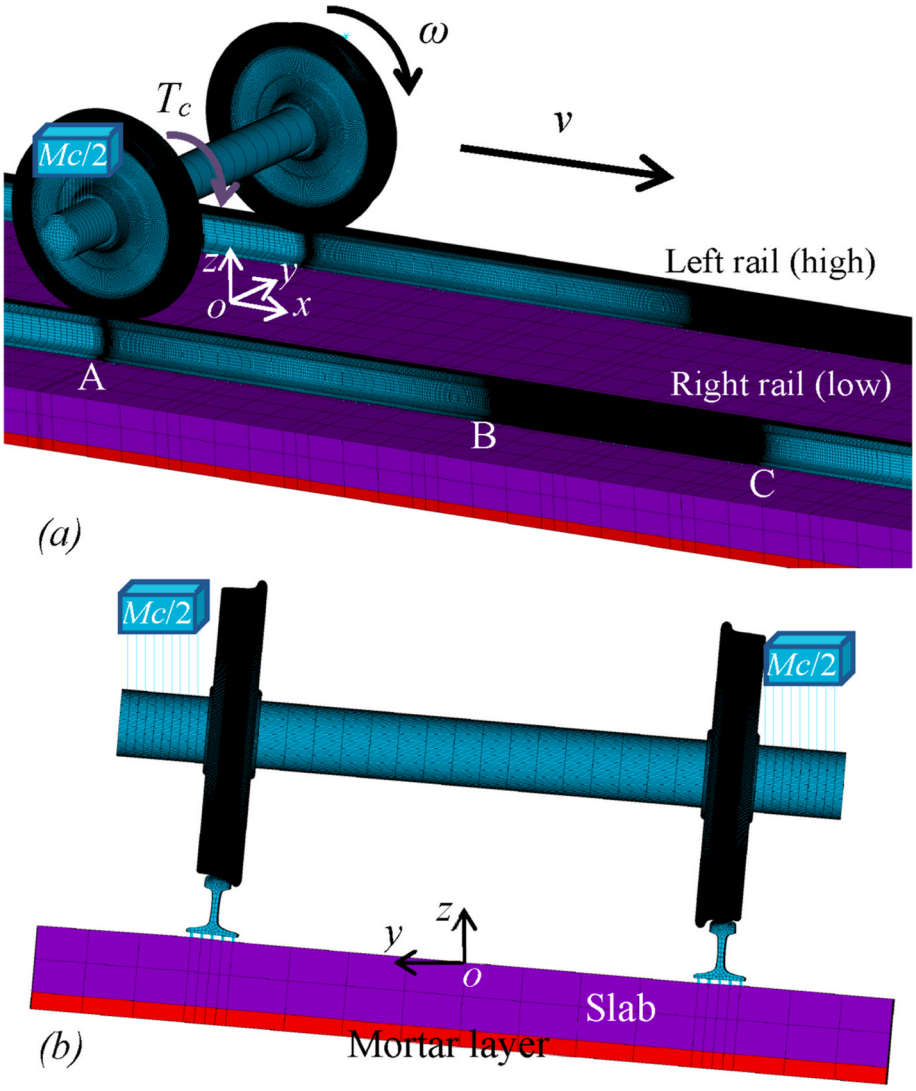

Fig. 2. Mesh of transient rolling contact model of curving.

Table 1
Steady lateral shift, roll and yaw angles of the leading wheelset running on a R7000 m curve calculated in SIMPACK.

Speed (km/h)	Lateral shift (mm)	Roll angle (°)	Yaw angle (°)
350	3.889	0.008 48	0.008 6
400	4.148	0.005 62	0.009 2
450	4.400	0.006 88	0.009 9
500	4.823	0.002 92	0.010 8

Table 2
Values of key parameters involved in the model.

Parameters			Values
Rolling speed, v (km/h)			≤500
Lumped sprung mass, m_c (kg)			13220
Wheel diameter, φ (m)			0.86
Wheelset mass, m_w (kg)			1019
Unsprung mass attached to wheel m_a (kg)			761
Primary suspension per side		Stiffness, K_p (kN/m)	880
		Damping, C_p (kNs/m)	4
Each rail fastening		Stiffness, K_f (kN/m)	22
		Damping, C_f (kNs/m)	200
COF	Dry		0.45
	LAZ	350 km/h	0.036
		400 km/h	0.032
		450 km/h	0.029
		500 km/h	0.027
Wheel & rail material		Young's modulus, E (GPa)	205.9
		Poisson's ratio, υ	0.3
		Density, ρ (kg/m^3)	7790
		Damping constant, β (s)	1.0×10^{-4}
		Yield strength, σ_Y (MPa)	450
		Tangent modulus, T (GPa)	21
Material of pre-fabricated slabs		Young's modulus, E_s (GPa)	34.5
		Poisson's ratio, υ_s	0.25
		Density, ρ_s (kg/m^3)	2400
Material filled in slab gaps		Young's modulus, E_g (GPa)	29.5
		Poisson's ratio, υ_g	0.25
		Density, ρ_g (kg/m^3)	2400
Mortar material		Young's modulus, E_m (GPa)	8
		Poisson's ratio, υ_m	0.2
		Density, ρ_m (kg/m^3)	1600

damage is usually found when measuring wheel roundness, e.g., before turning, it is rather hard or almost impossible to identify its cause by certain direct approaches, especially considering that a train runs up to 3000 km a day and their possibility of occurrence is rather low. Based on available information and previous research, the authors tend to believe that such long flats should originate from short LAZs, to be specific, from the irregular wear caused by short LAZs.

In a word, low adhesion is still an important problem for high-speed trains, especially in bad weather, even though with above mentioned countermeasures. In light of the key issue behind the above mentioned wheel damages, i.e., low adhesion, this work further develops the wheel-rail transient rolling contact model over short LAZs in Ref. [2] to study the dynamic/transient rolling contact of a wheelset in the presence of low adhesion. Considering that low adhesion caused by oil and anti-icing fluid leakage and dynamic unloading is more likely to occur on one side rail in reality, i.e., unilateral low adhesion, and low adhesion on both sides can approximately be simulated using half-wheelset model in Ref. [2] if tangent tracks are considered, focus of this work is placed on more complicated cases of high speed curving in the presence of unilateral short LAZs and the resulting irregular wear.

2. Modeling approach

2.1. Transient rolling contact model of curving

Following the modelling approach in Refs. [2,8], a transient rolling contact finite element (FE) model is developed for a Chinese high-speed railway in ANSYS/Ls-dyna, as illustrated in Fig. 2, to simulate the curving of a wheelset in the time domain at a speed up to 500 km/h. A whole wheelset and a section of curved slab track with discretely supported rail are simulated, so that the longitudinal and the lateral creepages and the spin can all be considered simultaneously. Vehicle components above the primary suspension, whose influences on high-frequency and transient wheel-rail interactions are insignificant, are simplified into unsprung mass m_c. A right curve with a radius of curvature of R7000 m (the minimum in 350 km/h high speed railway in China) and a super-elevation of 133 mm are considered, and the track is set to be 15.2 m long (include 24 fastenings). The rail, the fastenings, the slabs and the mortar layer are all included. The negligible influence of a longer track on the investigated results had been verified in the previous work by extending the simulated track [9].

A leading wheelset of a motor car that can meet LAZs more likely than trailing ones is considered, and its initial position and orientation with respect to the track is set by taking the steady lateral shift, roll and yaw angles calculated from vehicle dynamics analyses in SIMPACK, see Table 1 for their values at different speeds when irregularities are ignored. Actual geometries of the wheelset and rail are considered by a mesh of 8-node solid elements, in which LMa wheel profile matches CN60 rail profile with an inclination of 1:40. The axle load is taken as 15 t in consideration of the practice in Chinese high-speed rails. To solve the wheel-rail rolling contact, a surface-to-surface contact algorithm (by the penalty method) is employed with the Coulomb's law of friction. LAZs caused by water contamination is assumed, and the speed dependent coefficient of friction (COF) listed in Table 2 is taken according to the test results on a full-scale test rig [10]. For dry sections where contaminants are absent, the COF is set to be speed independent and taken as 0.45. All wheel-rail COFs are assumed to be constant, suggesting that the negative slope of creep curves after friction saturation is ignored. An explicit time integration scheme is employed for solution, resulting in a very short time step of 10^{-8}~10^{-7} s, hence, high frequency or transient contact phenomena can be obtained. For the slab and mortar layers, the mesh of 8-node solid elements is also applied and continuous mesh is assumed in their interface. Each fastening system is simulated by 12 groups of parallel springs and dampers distributed in the actual area of a rail pad, to be detailed, 3 columns in the longitudinal and 4 rows in the lateral. The total numbers of elements and nodes are 5.90 and 5.54 M, respectively.

Considering that the wheelset-track system is elastically deformed under normal service conditions, linear elastic material models are applied to all component. More accurate material models, once ready and if necessary, can easily be introduced due to the characteristics of the FE approach. Material damping of the wheel and rail is considered by the Rayleigh damping (C_m):

$$C_m = \alpha m + \beta K \tag{1}$$

where α and β are the mass (m) and the stiffness (K) proportional damping constants, respectively. In this work, the mass proportional damping is ignored because it is effective for low frequency vibrations. Value of β is taken based on estimate made by inverse modelling in Ref. [11]. Values of key parameters are given in Table 2.

In a simulation, the wheelset rolls forward along the rails with specified translational and rotational velocities and creepages, in which a time-dependent drive torque (T_c) is further applied to the wheel axle to simulate a traction case. Typically, a rolled distance of 3.4 m is simulated in each case, being longer than the circumference of wheel (2.7 m). The boundary conditions are set as follows: the bottom of the track or of the mortar layer is fixed, and symmetric boundary conditions to the track ends. The upper nodes of primary suspension are constrained with the corresponding lower ones along the longitudinal and lateral directions, and so are the rail fastenings. A right-handed Cartesian coordinate system attached to the track is defined, of which the origin O is

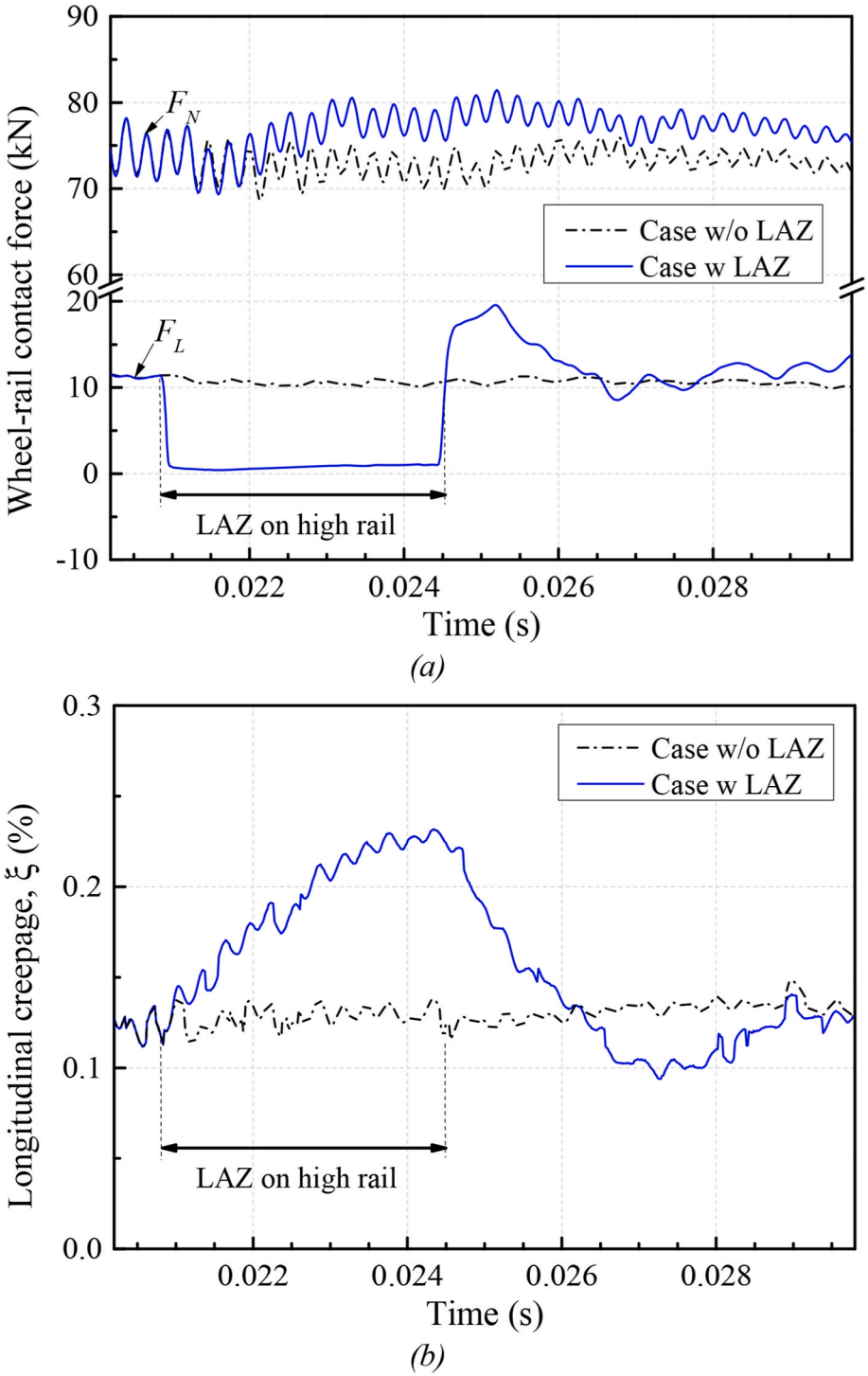

Fig. 3. Results on the high (left) rail side caused by a 0.4 m long LAZ on the high rail: a) Contact forces. (b) Longitudinal creepage.

located at the surface centre of slab under the initial position of the wheelset axle, and y axis along the lateral direction.

2.2. Wear model

The irregular wear around wheel caused by LAZs is calculated by a $T\gamma$ model developed for the high-speed wheel-rail system in Ref. [8], where T is the creep force and γ the creepage. The material loss at a surface node $m_{Tw}(x,y)$ (unit: μg) is determined by

$$m_{Tw}(x,y) = \int_0^t k^T A v dt = \sum_{i=1}^{n_t} k_i^T A v_i \Delta t_W \tag{2}$$

where, A, v and Δt_W are the area represented by the node (mm^2), the rolling speed (m/s), and the time step (s), respectively, subscript i corresponds to instant $i\Delta t_W$, and wear rate k^T (μg material loss/m rolled distance/mm^2 contact area) is a function of $T\gamma/A$.

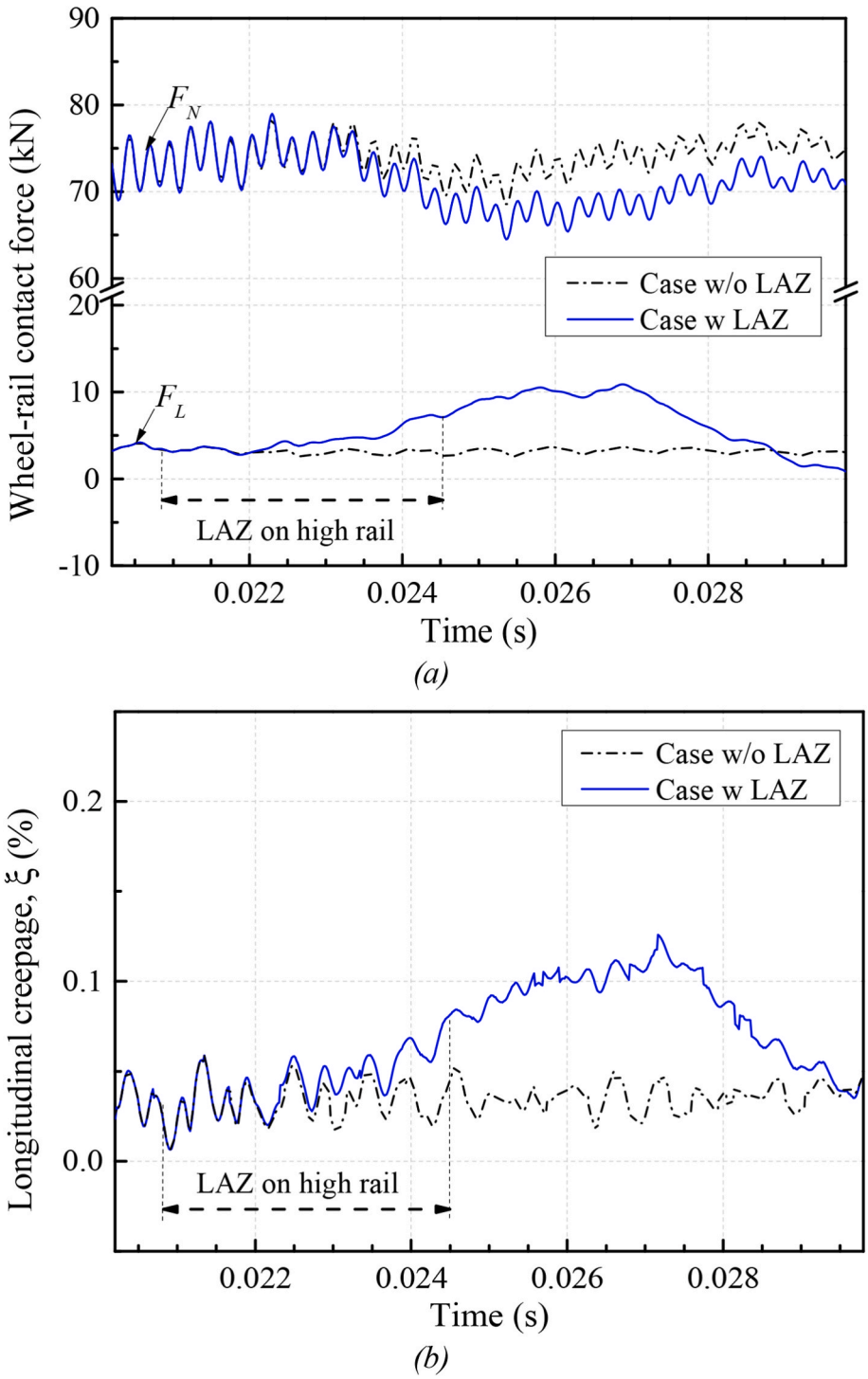

Fig. 4. Variations of contact force and longitudinal creepage on the low (right) rail side caused by a 0.4 m long LAZ on the high (left) rail: (a) Contact forces. (b) Longitudinal creepage.

$$k_i^T = k^T\left(\frac{T_i\gamma_i}{A}|(x,y)\right) = k^T\left(\tau_i\frac{s_i}{v_i}\right) \tag{3}$$

$$k_i^T = \begin{cases} 1.054\tau_i s_i/v_i \ (\tau_i s_i/v_i < 4.34) \\ 4.574 \ (\tau_i s_i/v_i \geq 4.34) \end{cases} \tag{4}$$

where, τ and s are the surface shear stress (MPa) and the sliding velocity (m/s) at the node.

3. Results of unilateral LAZs

3.1. Transient rolling contact and irregular wear

Following the approach in Ref. [2], a LAZ of 0.4 m length is applied on the high (left) rail to study its influence on transient wheel-rail rolling contact during curving. A speed of 400 km/h is assumed, a traction coefficient of 0.1 is taken to consider the worst case scenario [2], and the COF in LAZ is taken as 0.032 (see Table 1).

Fig. 3 shows the contact forces and the longitudinal creepage (ξ) on

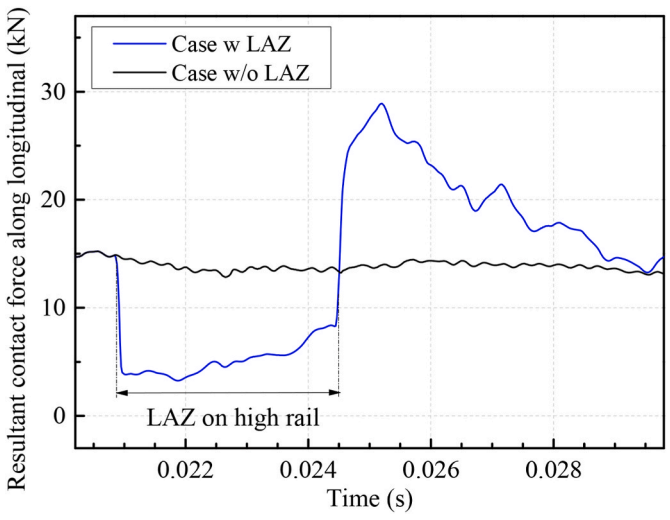

Fig. 5. Variations of the resultant contact forces along longitudinal caused by a 0.4 m long LAZ on the high (left) rail.

the high rail side where the LAZ is applied. The corresponding results of a case without the LAZ are also plotted in the figures as reference. It is seen that the longitudinal contact force (F_L) becomes clearly lower in the LAZ, resulting in imbalance between the friction torque and the drive one, and, thus, the wheel slip or creepage increases. As the wheel leaves the LAZ and re-enters dry rail, the longitudinal contact force first reaches a significantly higher level than the stable value in the reference case (19.6 kN Vs 10.7 kN), because of the creepage increase accumulated in the LAZ (0.23% Vs 0.13%), and then approaches the stable value gradually. These are similar to the results of half wheelset model reported in Ref. [2], except that the longitudinal contact force and creepage here may become lower than those of the reference case at certain instants after the LAZ. Moreover, Fig. 3(a) shows that the normal contact force (F_N) increases by 5 kN approximately in the simulated time period when the LAZ is present, which was not captured in Ref. [2]. Note that the normal direction here is approximately along the vertical, and the negligible lateral force is not presented. According to the widely accepted $T\gamma$ RCF model [12,13], the above mentioned larger contact force and creepage resulting from LAZs could explain the occurrence of wheel RCF in Fig. 1(a).

Fig. 4 shows the corresponding results on the low rail side where contact surface is continuously dry. Decrease of the normal contact force (F_N) by 5 kN approximately can be observed together with the increase of the longitudinal contact force and creepage, as the LAZ is present. These compensate the normal contact force increase and the drive force loss on the LAZ side (see Fig. 3). Since the creepage on the low rail side starts to increase about 1.5 ms later than the decrease on the LAZ side, the increase slope of the creepage curve in Fig. 3(b) starts to reduce from about 0.0225 s. At the trailing edge of the LAZ, the drive force increase on the low rail side is still insufficient to completely compensate the loss on the high rail side, as more clearly seen from Fig. 5 in which the summation of the longitudinal contact forces on both sides are shown. This means that the creepages and resultant longitudinal contact force would further increase in longer LAZs, as will be seen later. Moreover, after leaving the LAZ, the creepage on the high rail side starts to decrease immediately, while that on the low rail side continues increasing first and starts to decrease about 3.0 ms later. Note that within the presented time period, the resultant longitudinal contact force become always higher than that of the reference case after the LAZ (see Fig. 5), being in line with the results in Ref. [2].

To figure out the mechanisms of the above mentioned changes on two sides and time lags between each other, the bending and torsional vibrations of the wheelset caused by the LAZ are studied. First, variations of the vertical displacement of wheelset caused by the LAZ, i.e., the vertical displacement of the case with LAZ minus that of the case without, is derived for any instant from the results of two cases in Figs. 3–5. Fig. 6(a) shows the obtained distributions along the axis of the wheelset, in which each symbol represents a node on the axis. It is seen that after t2 instant the sudden reduction of the longitudinal contact force on the left side (due to LAZ) results in a bending vibration starting from the left side and propagating towards the right side. When the left wheel leaves the LAZ (at an instant slightly before t6), the restored longitudinal contact force further modifies the bending deformation and forces it back to the original state before the LAZ gradually (such a recovery process is relatively long, and not simulated completely here). Looking at the result at t7 when the bending deformation has been built up, the left wheel moves downward because of the LAZ, explaining the normal contact force increase there (see Fig. 3(a)). Correspondingly, upward movement of the right wheel explains the decrease of the normal contact force in Fig. 4(a).

Fig. 6(b) shows distributions of the rotational speed of the wheelset along its axis at the same instants. It is seen that the rotational speed is constant along the axis before the LAZ or at t1 and t2 instants. When the left wheel enters the LAZ, i.e., after t2, the rotational speed of the left wheel starts to increase owing to creepage increase in the LAZ, and such increase gradually propagates toward the right wheel. At t6 an approximately even distribution along the axis but at a higher rotational speed is reached. In other words, torsional vibrations of the wheelset are excited by the sudden changes of longitudinal contact forces on both sides, and transmit between two wheels. Afterwards, due to restoration of the longitudinal contact forces after the LAZ, the wheelset is excited torsionally again, under which the rotational speed changes back to the original state before the LAZ gradually and the left side recovers first as well. Transmission of the bending and torsional vibrations between two wheels is the reason why time lags are present between the results on two sides in Figs. 3 and 4. Note that the y coordinate of the axis centre is less than zero, as shown in Fig. 6, because of the superelevation of the curved track. The lateral position of the wheelset changes with time during curving, but un-noticeable among the instants in Fig. 6 because of large radius and short time period presented.

Fig. 7 further shows the out-of-roundness of two wheels after one cycle of rolling in a polar coordinate system, in which cases with and without the LAZ are both plotted for comparison. For clarity, only 2D results passing the location of maximum pressure in a contact patch are shown. In simulations, the contact patch moves counter-clockwise around the wheels, and the left wheel enters the LAZ at about 230°. From the results of the left wheel in Fig. 7(a), it is seen that a plateau occurs on the part contacting the LAZ owing to reduced wear rate, after which a hollow first follows due to increased longitudinal contact force and accumulated creepage there (see Fig. 3), and then converges to the result of the case without LAZ gradually. The hollow may be considered as a small wheel flat. In contrast, a much wider hollow occurs on the right wheel because of the LAZ, corresponding to the results in Fig. 4, i.e., a large wheel flat. The maximum radius difference around wheel, resulting from the LAZ, is 5.4×10^{-7} and 4.6×10^{-7} mm for the left and right wheels, respectively. Note that zero in the roughness axis is defined on the worn surface of the left wheel, so that the right (low side) wheel is larger due to less wear determined by less contact force and creepage during curving.

3.2. *Influence of the LAZ length*

Besides the LAZ length of 0.4 m considered last section, more lengths of 0.2, 0.6, 0.8 and 1.0 m on the high rail are simulated in this section, for which all other parameters are kept unchanged. Fig. 8 shows variations of the longitudinal contact force and creepage on both sides when the length varies from 0.2 to 1.0 m. For easy comparison, all LAZs are set to end at the same location, and the starting position varies. Fig. 9 further shows variations of the resultant contact force along the

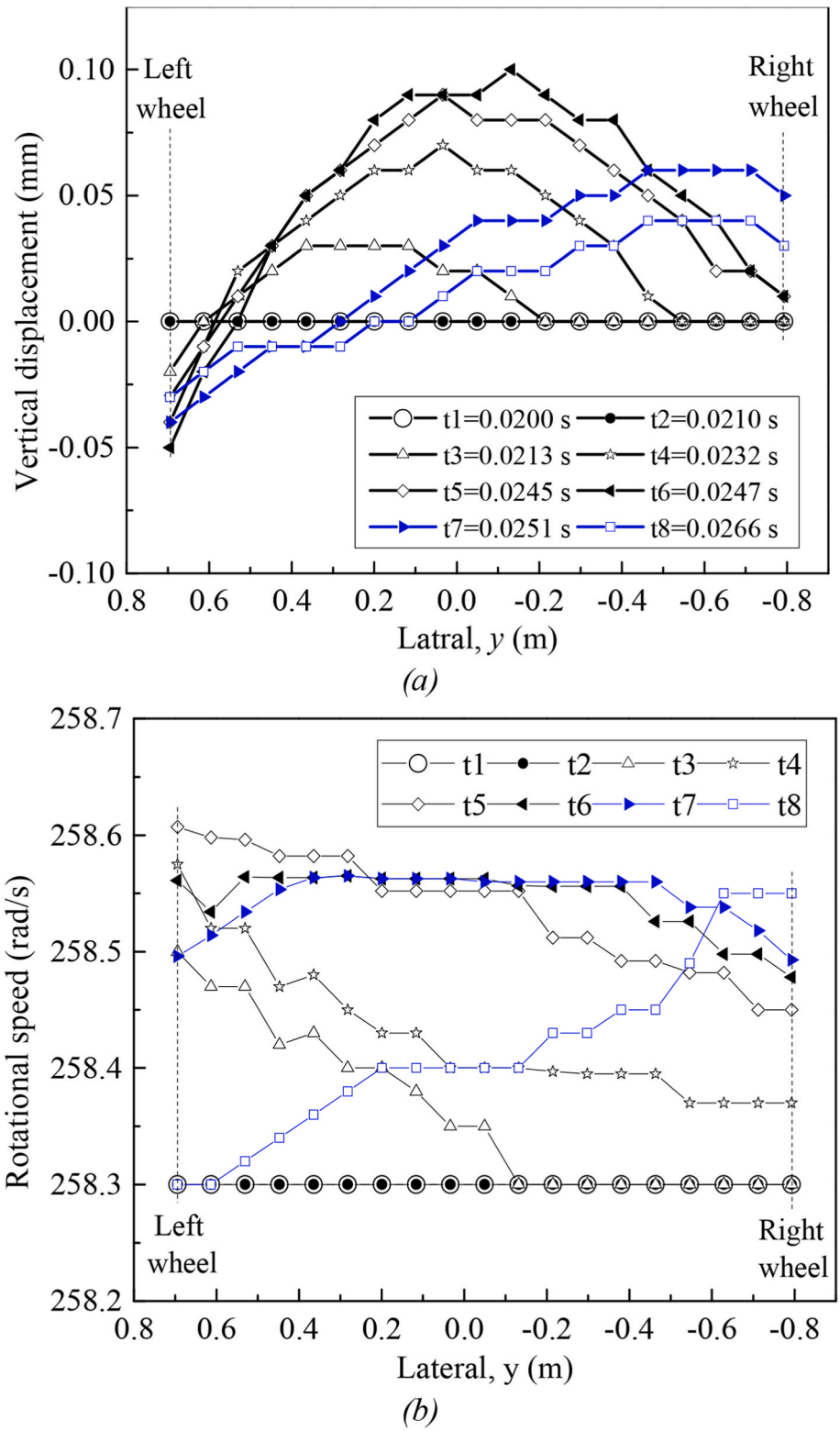

Fig. 6. Dynamic deformation and motion along the wheelset axis when passing a 0.4 m long LAZ on the high (left) rail: (a) The vertical displacement caused by the LAZ. (b) The rotational speed.

longitudinal. Note that normal contact forces are not plotted in Fig. 8 because their changes about 5 kN do not vary considerably with the length of LAZ.

From Fig. 9 it is seen that as the LAZ is slightly longer than 0.6 m, the resultant contact force in the LAZ gradually increases to the level of the case without LAZ, i.e., the increase on the low rail side can completely compensate the loss on the high rail side. At a longer LAZ, worse wheel idling will not occur within the LAZ, see the results of the 1.0 m long LAZ. This means that for the adhesion situation considered in this section, unilateral low adhesion just leads to redistribution of drive force between two wheels by increasing the creepages on both sides (see Fig. 8), and does not cause idling of the whole wheelset. Such a

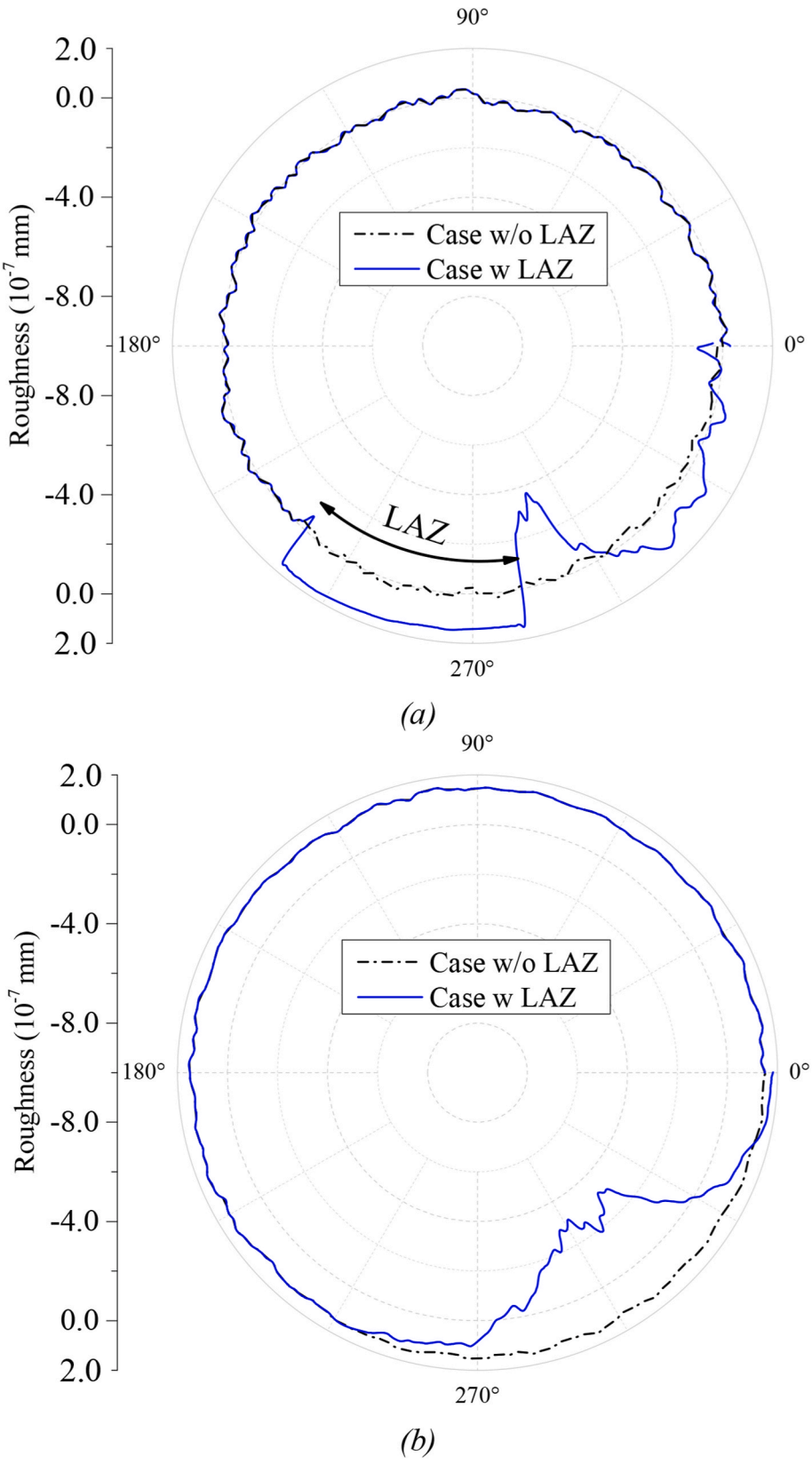

Fig. 7. Out-of-roundness of wheels resulting from irregular wear when passing a 0.4 m long LAZ on high (left) rail: (a) Left. (b) Right.

redistribution determined by transmission of the bending and torsional vibrations lasts about 0.006 s, corresponding to a critical rolled distance or LAZ length of 0.66 m for the speed of 400 km/h and the traction coefficient of 0.1. After the redistribution, the longitudinal force and creepage both becomes approximately stable within LAZs. Moreover, once a LAZ is longer than the critical length, the recovery process after the LAZ becomes the same, as illustrated in Figs. 8 and 9, resulting in a maximum resultant force of about 30.0 kN (the corresponding force is

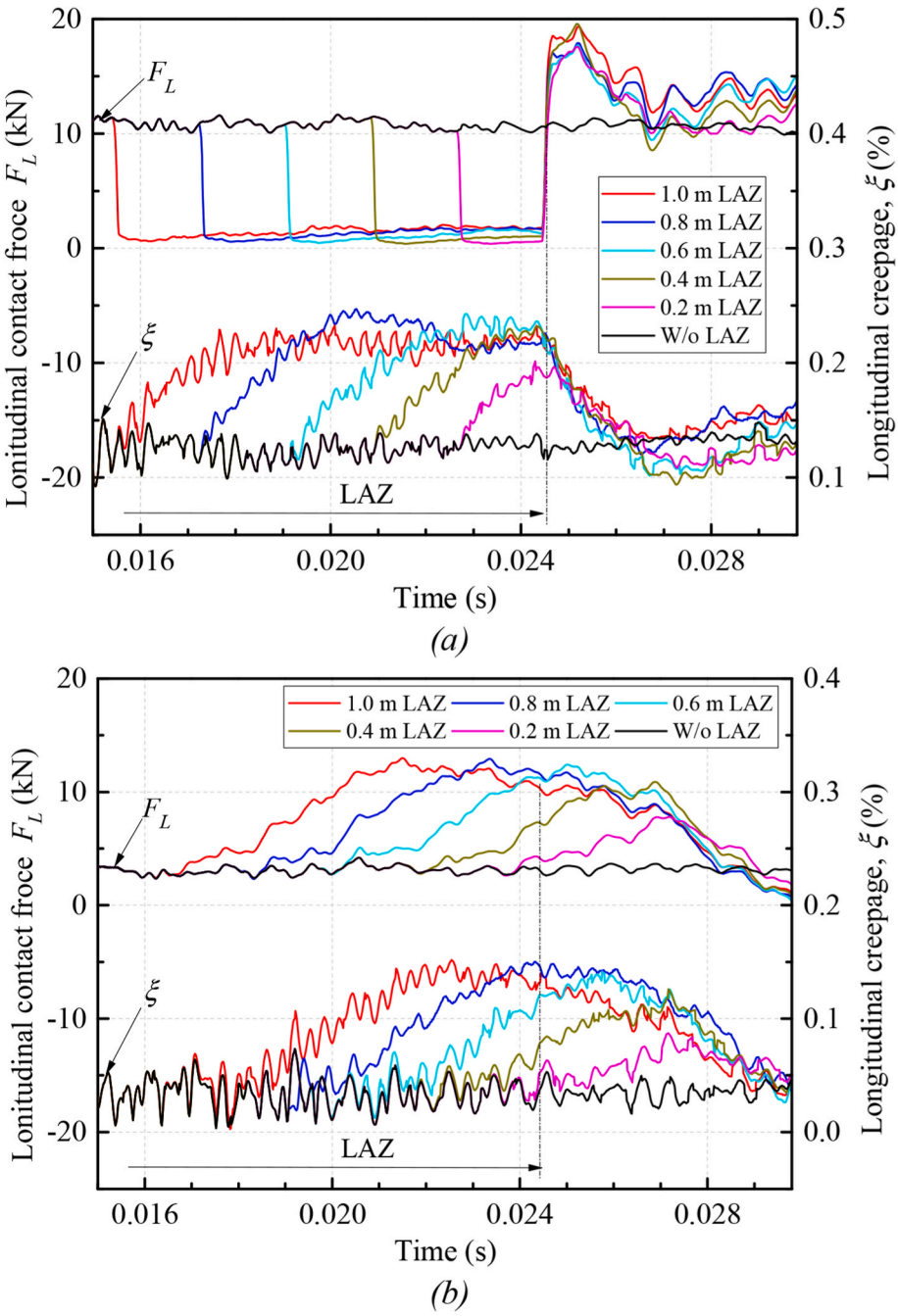

Fig. 8. Variations of the longitudinal contact force and creepage caused by LAZs of different lengths on high (left) rail: (a) Left side. (b) Right side.

about 14 kN when LAZs are absent). It is worthwhile to mention that the decrease of the longitudinal contact force on the high rail side and the increase on the low rail side would lead to a reduced curving torque, worsening the curving behaviour of the driving wheelset.

Fig. 10 shows out-of-roundness of two wheels when LAZs of different lengths are present on the high rail, for which one cycle of rolling is considered as well for all cases. It is seen that on the left wheel the plateau enlarges with the LAZ length, but the small wheel flat and the irregular wear pattern after the LAZs does not vary much. On the right wheel, however, the large wheel flat becomes larger with the LAZ length, and its depth first increases before the critical length of 0.66 m and then states approximately constant. The maximum radius difference is up to 5.5×10^{-7} mm and 6.7×10^{-7} mm for the left and right wheels, respectively. These suggests that a small flat like that in Fig. 1(b) may be triggered on the left wheel in low adhesion, while large ones may occur on the right one where adhesion is sufficient. It can further be imagined that if a LAZ is comparable to or longer than the wheel circumference, large flats will not be observed on the right wheel, and higher wear rate around the wheel is left behind instead. In other words, flats may not occur in pair on two wheels of a wheelset.

3.3. LAZ on high rail vs. on low rail

LAZs of different lengths are applied on the low rail in this section to study their influences. Except for the application side, all other parameters are kept the same as those in section 3.2, including LAZ lengths and their ending position, for comparison with cases above. The normal contact force is found to increase on the low rail side, and decrease on the high rail side. Considering the results above, it can be concluded that unilateral low adhesion would lead to increase of the normal contact

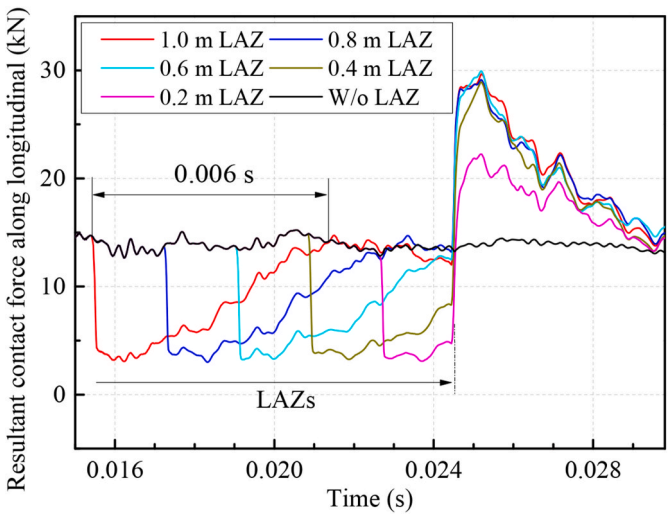

Fig. 9. Variations of the resultant contact force along longitudinal caused by LAZ of different lengths on the high (left) rail.

force on the low adhesion side, and decrease on the other. Corresponding normal contact forces are not given here since they are out of the core objective of this work.

Fig. 11 shows variations of the resultant longitudinal contact force when the same LAZs are separately applied on two rails. For clarity, only two lengths of 1.0 and 0.6 m are included. It is seen that the trend is similar for LAZs on two rails, but the magnitudes are significantly lower in the cases with LAZs on the low rail. For example, when applied to the low and the high rail, the maximum longitudinal forces (indicated by downward arrows in the figure.) are 18.9 kN and 30.0 kN, respectively. This is because the longitudinal force is larger on the high rail than that on the low rail during curving (see Fig. 8), and the same contamination would result in more severe adhesion insufficiency or low adhesion when occurring on the high rail (see Fig. 11).

Fig. 12 further shows the maximum longitudinal contact force and creepage versus the length of LAZ when LAZs are separately applied on two rails. Similar trends and significantly different magnitudes are clearly shown. Note that the critical length of 0.66 m derived from cases with LAZs on the high rail is still valid for LAZs on the low rail, as seen from Figs. 11 and 12, suggesting the same time lags between results of two sides. In terms of the resulting out-of-roundness of wheels, the trend is also similar, i.e., small and large flats are expected on the low and the normal adhesion sides, respectively, but lower magnitudes are present when the LAZs are on the low rail (corresponding results are omitted here due to limited space).

4. Influence of speed and COF

Above, the speed is set as 400 km/h and a COF of 0.45 is taken for zones out of LAZs. In this section, the speed is first varied between 350 and 500 km/h to analyze its influence, for which the COF in LAZs varies as listed in Table 2. Then, the COF out of LAZs is changed down to 0.15 in consideration of random contaminations in field. In these cases, a 1.0 m long LAZ is assumed, and is applied on the high rail to simulate more detrimental situations. All other parameters are kept unchanged.

From Fig. 13(c) it is seen that the critical length of LAZ increases with speed, i.e., the recovery of the resultant longitudinal contact force to the required level in the LAZ needs a longer rolled distance at a higher speed. This is due to fixed frequencies of the bending and torsional vibrations of the wheelset that determine the time period of the longitudinal force redistribution between two wheels. Due to similar reasons, the recovery after the LAZ also realizes within a longer distance at a higher speed. Fig. 13(a) and (b) shows the decomposed results on both sides. It is seen that on the LAZ or left side, the longitudinal contact force does not change much with the speed, while the creepage stabilizes to a lower value at a higher speed, resulting in a lower creepage at the end of the LAZ. On the low rail side, the stabilizations of the longitudinal contact force and creepage in the LAZ and the attenuation after it all correspond longer distances at higher speeds, and their maximums during the whole process decrease noticeably with speed. Consequently, the resulting irregular wear on wheels (i.e., the wheel out-of-roundness) decreases considerably in magnitude with speed, as shown in Fig. 13(d).

Keeping 400 km/h and a 1.0 m long LAZ on the high rail, the influence of the COF out of the LAZ is shown in Fig. 14. It is first seen from Fig. 14 (a) and (b) that before the LAZ (under the state of approximately steady curving) the longitudinal contact force increases slightly with the COF on the high rail, while decreases correspondingly on the low rail. This is because its component caused by curving is forward on the high rail, backward on the low, and their magnitudes mainly determined by the rolling radius difference between two wheels increase with the COF. When combining with the component caused by driving, being forward in direction, the above mentioned phenomenon could be explained. Moreover, because a constant drive torque is applied, the resultant longitudinal force of the wheelset does not change noticeably before the LAZ (Fig. 14(c)). Note that the corresponding creepages on two sides both decrease slightly with the COF (Fig. 14 (a) and (b)).

When entering the LAZ, the resultant force applied to the wheelset first decrease suddenly from about 14 kN to even below 4 kN, and then gradually reaches stabilized levels, as shown in Fig. 14(c). As the COF decreases, especially below 0.25, the sudden change becomes less severe because of smaller COF difference across the LAZ, resulting in larger resultant force in the leading part of the LAZ and lower stabilized force in the trailing. The stabilized forces show that the adhesion on the low rail is sufficient to completely compensate the drive force loss on the high rail, when the COF is larger than or equal to 0.25. For lower COFs, however, the torque imbalance becomes to exist throughout the LAZ, thus, the critical LAZ length is absent and the creepages on two sides both increase continuously in the LAZ, as seen from Fig. 14 (a) and (b). In other words, obvious wheelset idling would occur when the COF out of the LAZ is low enough and the LAZ is sufficiently long. Fig. 14 (a) and (b) further show that in the LAZ the influence of the COF on the longitudinal contact force of the right side is similar in trend to its influence on the resultant force in Fig. 14(c), while on that of the left side is negligible. This means that the resultant force in the LAZ is dominated by the component on the low rail, being easy to understand.

When leaving the LAZ, the resultant force reduces in magnitude with the decrease of the COF (Fig. 14(c)). Looking at the longitudinal contact forces after the LAZ on two sides in Fig. 14(a) and (b), it is found that the force on the high rail, with respect to that on the low rail, plays a more important role in the resultant force. Furthermore, the corresponding creepage increases with the decrease of COF, being in line with the creepages in LAZs, and its decreasing rate reduces correspondingly. These suggest that the recovery to the stable rolling before the LAZ is more difficult as the COF out of the LAZ is lower.

From wear distributions around two wheels in Fig. 14(d), it is seen that the magnitude of the resulting irregular wear increases on the left wheel as the COF decreases, while that on the right wheel does not change much correspondingly, especially for the COFs larger than 0.2. Note that the irregular wear is plotted in a Cartesian coordinate system in the figure for convenience instead of a polar coordinate system used above.

5. Discussions

It should be noted that in this work many complicated and variable factors exiting in practice are simplified properly, according to the authors' best understanding, to manifest the importance of low adhesion and avoid unnecessary difficulties in analyses. Short LAZs considered in this work are found to be long enough for analyses of unilateral low

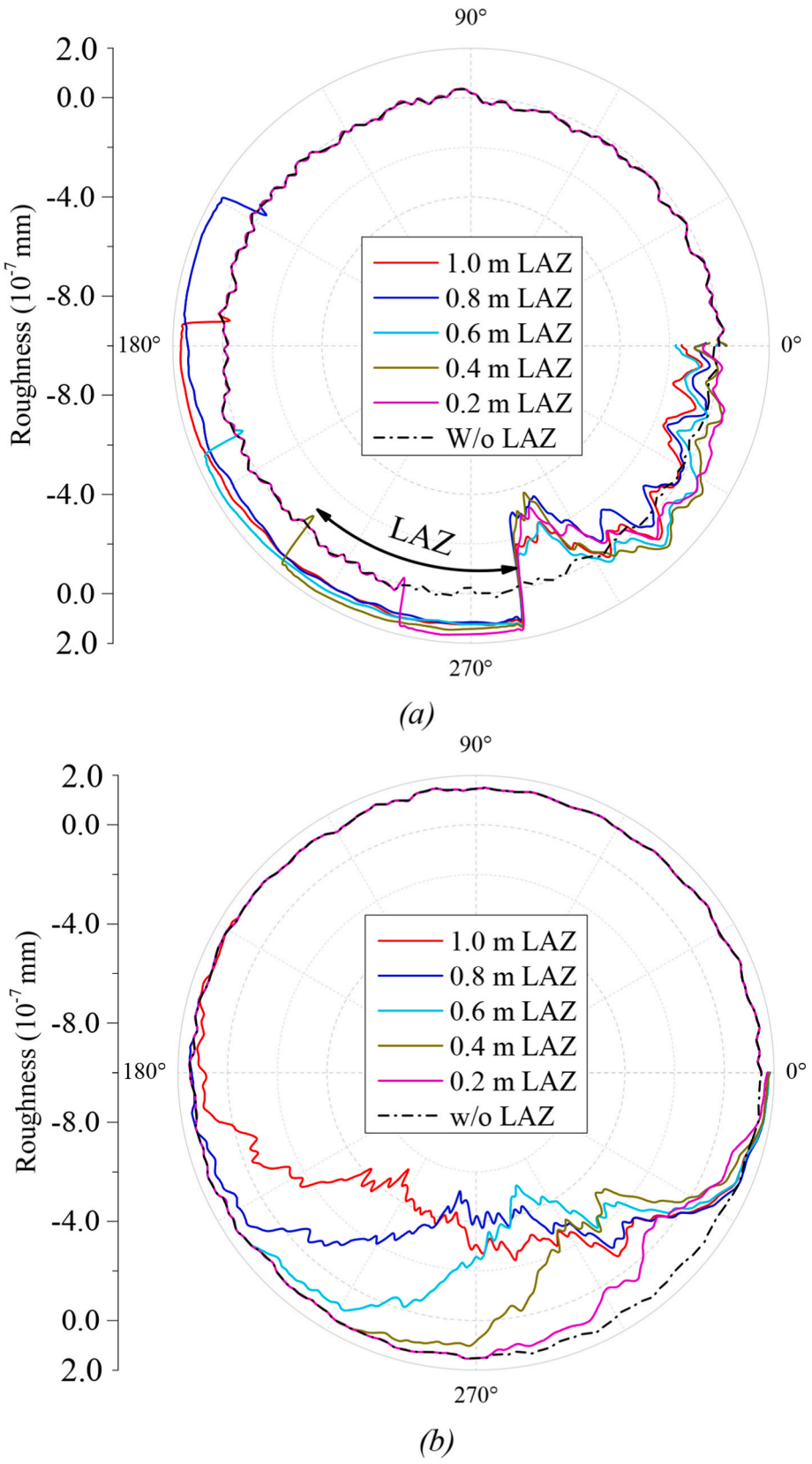

Fig. 10. Out-of-roundness of wheels caused by LAZs of different lengths on the high (left) rail: (a) Left. (b) Right.

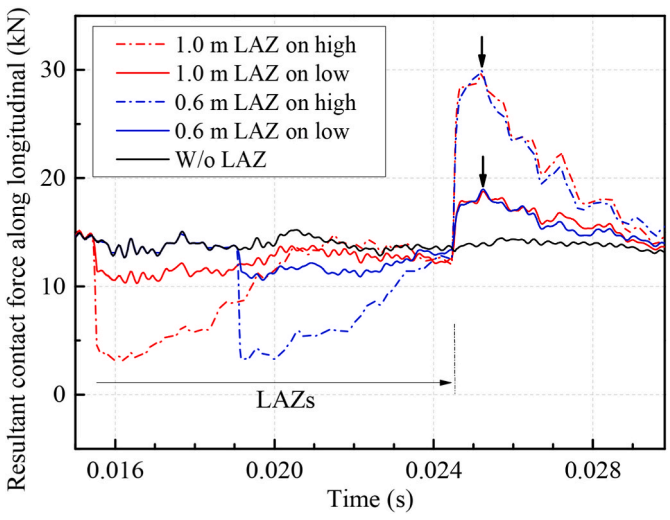

Fig. 11. Variations of the resultant contact force along longitudinal when LAZs are separately applied on high (left) and low (right) rail.

adhesion, where a force re-distribution occurs between two sides in the presence of low adhesion and is realized in the very short time period. Based on the results shown above, some discussions on the relationships between wheel damages in Fig. 1 and LAZs are given in the following. This can provide meaning information for further numerical or experimental studies on the damages, where more factors can be included, and the causes could be confirmed by more direct evidences. Note that no evidence has been collected from tracks because very limited tracks can be checked on foot at window times (typically 0–4 a.m.) and low possibility of occurrence of typically temporary low adhesion.

5.1. On wheel flats and LAZ

It is shown above that unilateral low adhesion would probably not result in significant idling of a wheelset, but can lead to slight increase of creepage and considerable irregular wear on both wheels. Due to transmissions of bending and torsional vibrations in the system and the drive/brake force redistribution between two sides, the wear pattern is significantly different on two wheels of a wheelset. Taking the cases in Section 3.2 for examples, where LAZs of different lengths are present on the high rail, relatively short flats could occur on the wheel passing the LAZs and their lengths are approximately independent of the length of the LAZ, on the other wheel, however, much longer flats occur and their lengths increase with the length of LAZ. To the authors' best guess, the flat in Fig. 1(b) should be a consequence of a short LAZ passed by the wheel, and the corresponding flat on the other wheel of the same wheelset is unrecogonisible due to its large length (i.e., unlike a flat), especially when the LAZ is longer than the wheel circumference. This explains the above mentioned phenomenon that a flat is visible on one wheel of a wheelset, but no corresponding one on the other. Note that flats resulting from short LAZs are very shallow, being unlike those observed in field. According to simulations of wear development over time in Ref. [14], defects like the shallow flats can gradually grow up during service, and lead to severe problems like that in Fig. 1(b) at the end. Such a mechanism is significantly different from the traditional understanding that flats usually occur in pair on two wheels of a wheelset, and may be with different severities [15].

It worth mentioning that the increased creepage over short unilateral LAZs, being less than 0.25% for cases in section 3.2, is far below the thresholds for operations of TC and WSP systems. Thus, the above mentioned mechanism also supports Stone's [16] deduction that flats may also occur under normal braking operations (results of normal braking cases are similar to those of normal driving cases shown above, but with creepages in the opposite direction). If low adhesion occurs on both sides, it can be expected that stable rolling will not be achieved by redistribution of the drive/brake forces between two wheels (see Ref. [2]), thus, creepages can increase to levels triggering the TC and WSP systems. If the TC and WSP systems do not operate appropriately or malfunction, flats in pair may come into being. Such a mechanism of wheel flats should be in line with the traditional understanding.

Two mechanisms above both show that low adhesion is the root cause of wheel flats. Therefore, results above and those in Ref. [2] can help explain the widely reported phenomenon that flats are more likely to occur when interface contaminants like fallen leaves, leaked oil and snow are present [17–20]. It should be noted that LAZs less than the wheel circumference is studied in this work to derive the critical LAZ lengths and avoid unnecessary difficulties related to superposition of different rolling cycles of a wheelset. Additionally, in consideration of superposition of numerous cycles and random wear around wheels caused by complicated service conditions, the irregular wear resulting from short LAZs may only be a problem when its magnitude is sufficiently high. This could be the reason why the defect in Fig. 1(b) is not widespread, which needs further studies.

5.2. On wheel RCF and LAZ

As mentioned in section 3.1, the widely accepted $T\gamma$ RCF model implies that larger contact force and creepage after LAZs, i.e., larger $T\gamma$ there, means higher possibilities of RCF occurrence when $T\gamma$ is less than a threshold of severe wear (it is so for cases considered in this work). Thus, results in this work indicate that RCF is more prone to occur when unilateral LAZs are present, even though stable rolling is reached very soon (no complete wheel idling occurs). If low adhesion occurs on both sides, creepage of the wheelset will increase further with respect to that in the unilateral cases, i.e., significant wheel idling may occur and more severe RCF is expected after the LAZs. Only when the LAZs on both sides are long enough, the creepage may increase to a level higher than the thresholds of TC and WSP systems, and triggers their operations. These are why anti-slip control operations were absent for a few wheelsets damaged by RCF in the heavy snow (Fig. 1(a)), and not continuous for other damaged wheels.

5.3. On counter measures of short LAZs

Regarding short LAZs considered above, a wheelset can pass it in a very short time period, e.g., lasting 9 ms in a 1.0 m LAZ at 400 km/h. Further considering that a stable rolling can be built up in a unilateral LAZ within 6 ms (Fig. 9), and the resulting creepage increase is very limited (Fig. 8), TC/WSP systems seem not take operations quickly and accurately enough. This is even true under dynamic and complicated conditions in practice, where all related parameters may vary in seemingly random ways, and mis-operations and too frequent operations have to be minimized. Therefore, it could not be a good idea to improve control systems against short LAZs, especially unilateral ones. However, control systems may be improved to better treat long LAZs present on both sides, e.g., by optimizing the thresholds and strategies of anti-slip operations, to avoid severe RCF problems and flats.

Assuming irregular wear and RCF damages from short LAZs are inevitable, some measures can still be taken to control the damages under a problematic level. To the authors' best understanding, tread trimmers is a feasible way, and its effectiveness on removal of wheel out-of-roundness and RCF cracks has been confirmed in practice [21]. The key to the success of a tread trimmer is to optimize a suitable strategy for short LAZs and determine the related key parameters. Another way against short LAZs is to apply adhesion enhancement preventively, for which sands, friction modifiers and so on can be used. Considering the limited amount of enhancement carried by a train, a critical state over which enhancement spraying should be triggered and the optimal spraying amount have to be determined first.

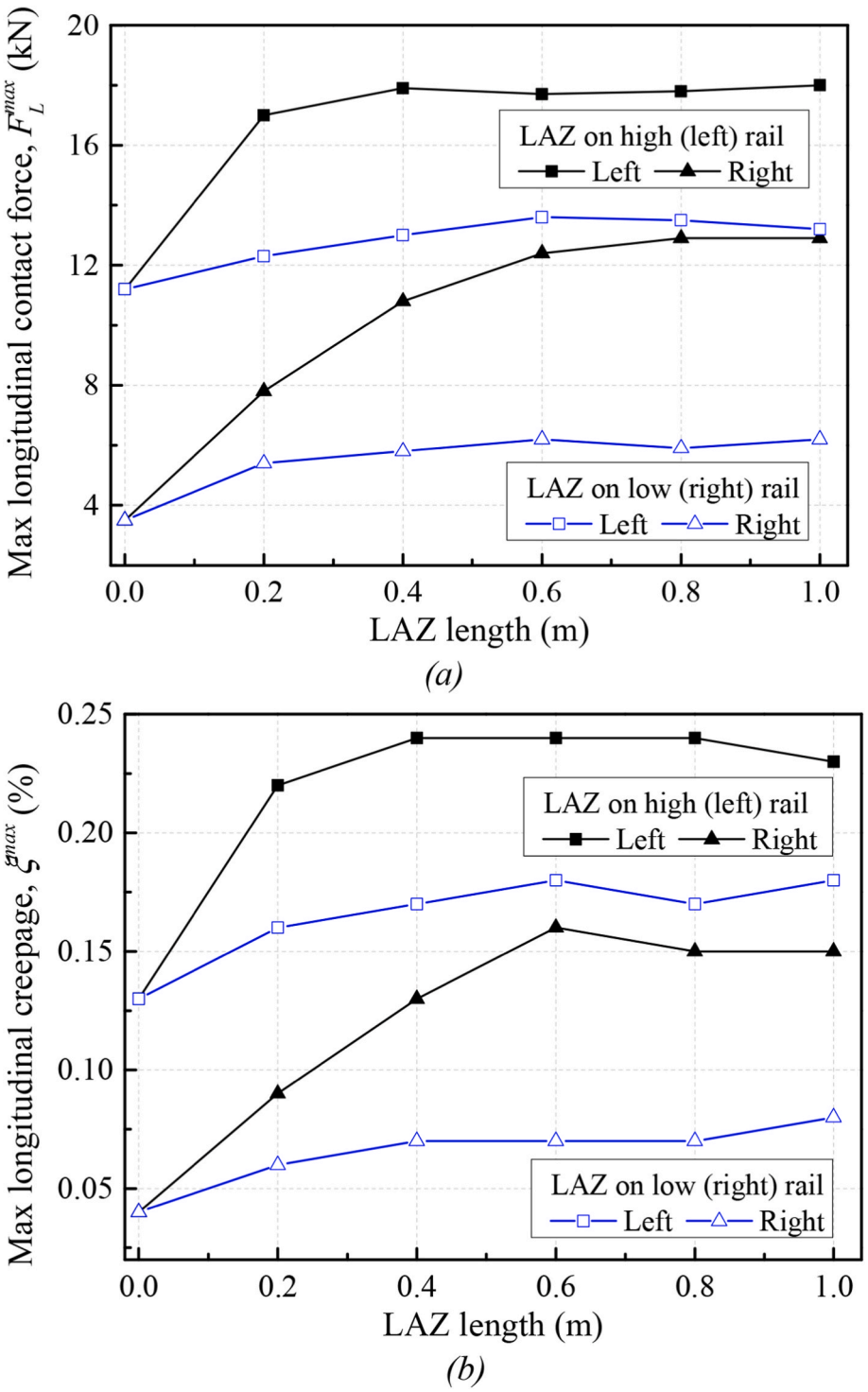

Fig. 12. Variations of the maximums with the length of LAZ: (a) The maximum longitudinal contact force. (b) The maximum longitudinal creepage.

6. Conclusions

A transient rolling contact model is developed to study the dynamic curving of a driving wheelset over a curved track at high speeds and in the presence of short unilateral LAZs. The length of LAZ is set to be 0.2–1.0 m, and the speed changes from 350 km/h to 500 km/h. COF in the LAZs is taken according to test results, and that out of the LAZs is varied between 0.15 and 0.45. From dynamic contact forces, creepages and deformations, and the resulting irregular wear, following conclusions are drawn.

1) When COF out of the LAZs is larger than or equal to 0.25, unilateral LAZs just result in slight increases of creepages on both sides, and no significant wheel idling occurs. The drive force loss on the low adhesion side is compensated completely by the increase on the other side. Such a redistribution process of drive force lasts about 0.006 s that is determined by transmission of the bending and torsional vibrations of the wheelset between two sides and corresponds to a critical LAZ length of 0.66 m at 400 km/h. LAZs on high rail are found more detrimental than those on low rail due to higher

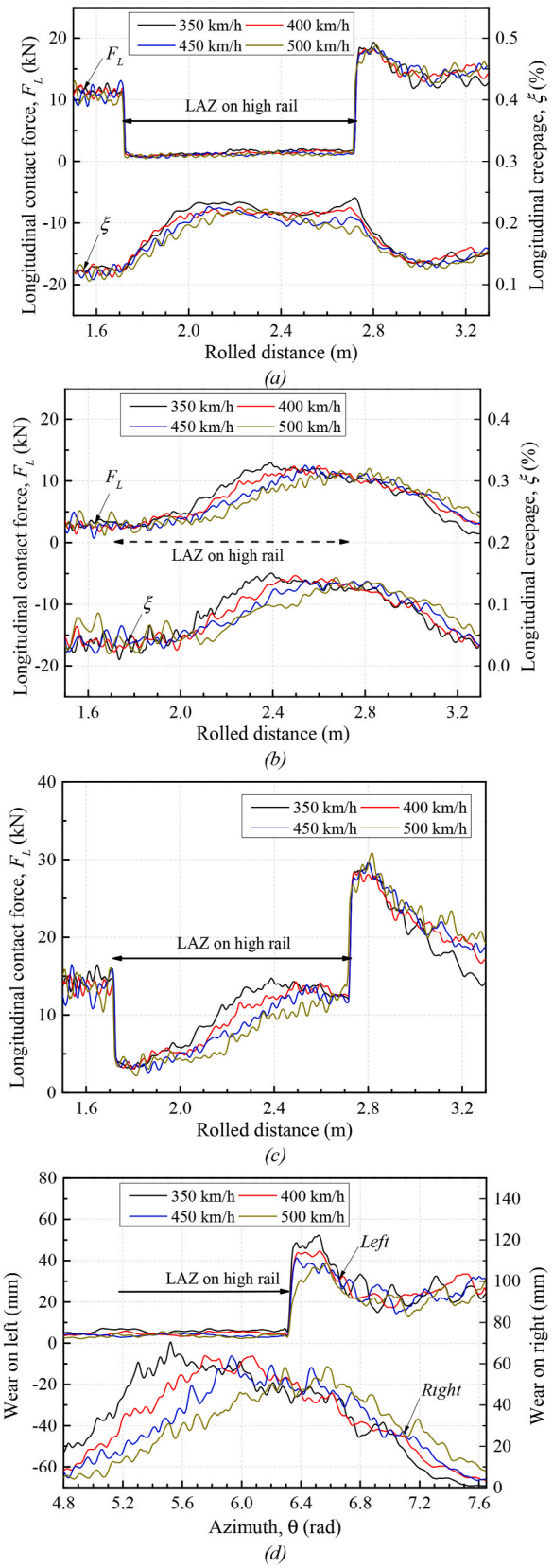

Fig. 13. Influence of speed under a traction coefficient of 0.1 when a 1.0 m long LAZ occurs on the high (left) rail: (a) The longitudinal contact force and creepage on the left side. (b) The longitudinal contact force and creepage on the right side. (c) The resultant longitudinal contact force. (d) The resulting irregular wear around wheels.

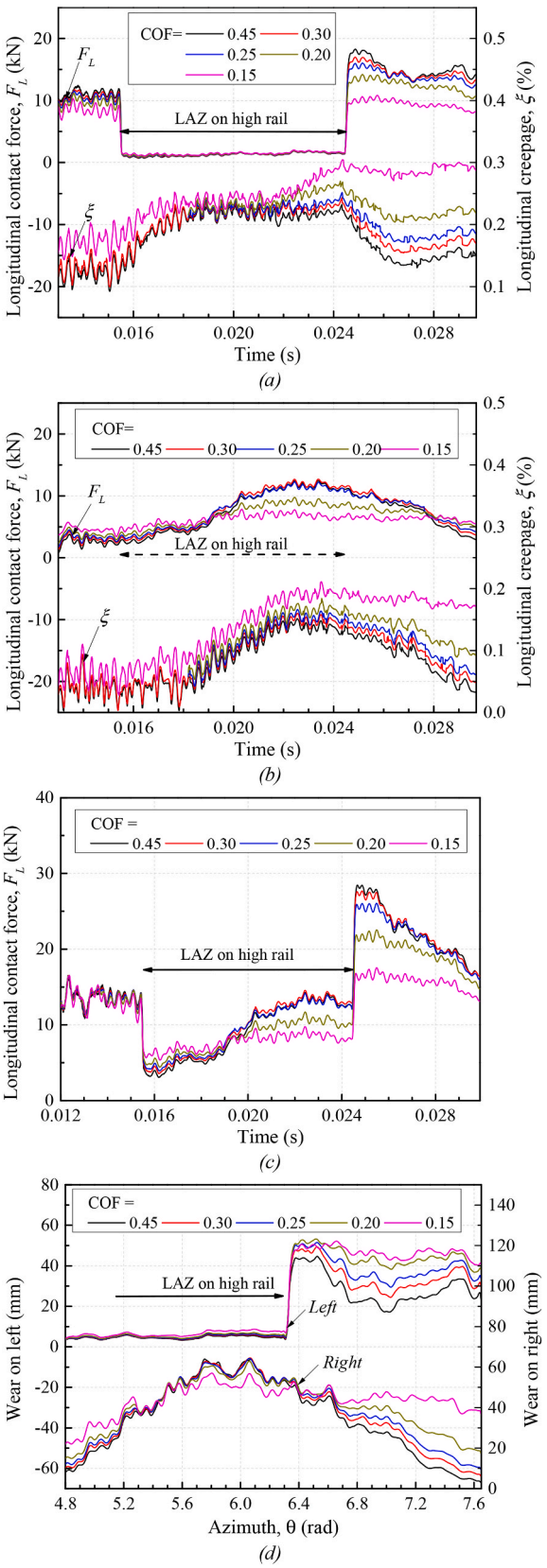

Fig. 14. Influence of the COF out of the LAZ at 400 km/h when a 1.0 m long LAZ occurs on the high (left) rail: (a) The longitudinal contact force and creepage on the left side. (b) The longitudinal contact force and creepage on the right side. (c) The resultant longitudinal contact force. (d) The resulting irregular wear around wheels.

requirement of drive force. The critical LAZ length increases with speed, and vanishes as COF out of the LAZs is less than 0.25.
2) Increased longitudinal contact force and creepage after LAZs explains why severe wheel RCF was widely observed after running in bad weather. The prediction of no significant idling explains the phenomenon that anti-slip control operations were absent for a few wheelsets damaged by RCF.
3) Short unilateral LAZs result in a short flat on the wheel of low adhesion side, and a larger one on the other whose length increases with the length of LAZ. As LAZs longer than the wheel circumference are present, flats are only expected on the low adhesion side, which explains the observation that flats just occurs on one wheel of a wheelset.
4) It seems infeasible to improve TC/WSP systems against short LAZs, especially unilateral ones. Optimized tread trimmers and preventive adhesion enhancement are possible countermeasures.

Declaration of competing interest

This manuscript has not been published or presented elsewhere in part or in entirety, and is not under consideration by another journal. All the authors have approved the manuscript and agree with submission to your esteemed journal. The authors declare that there are no conflicts of interest to declare.

Data availability

Data will be made available on request.

Acknowledgments

The present work is supported by the Science & Technology Research Program of Sichuan Province (2021YFH0006), and the Autonomous Research Project of State Key Lab of Traction Power (2022TPL-T06).

References

[1] O. Arias-Cuevas, Low Adhesion in the Wheel–Rail Contact, TU Delft, The Netherlands, 2010.
[2] X. Zhao, Z. Wen, M. Zhu, X. Jin, A Study on High-speed rolling contact between a wheel and a contaminated Rail, Veh. Syst. Dyn. 52 (10) (2014) 1270–1287.
[3] H. Chen, T. Furuya, S. Fukagai, et al., Wheel slip/slide and low adhesion cause by fallen leaves, Wear 446–447 (1) (2020), 203187.
[4] RAIB, Department for Transport, Collision at exeter st davids etation 4 january 2010, Rail Accident Rep. 10 (2010).
[5] RAIB, Department for Transport, Buffer stop collision at Chester station 20 November 2013, Rail Accident Rep. 26 (2014).
[6] K. Ishizaka, S.R. Lewis, R. Lewis, The low adhesion problem due to leaf contamination in the Wheel/Rail Contact: bonding and Low Adhesion Mechanisms, Wear 378–379 (1) (2017) 183–197.
[7] W. Wang, T. Liu, H. Wang, et al., Influence of friction modifiers on improving adhesion and surface damage of wheel/rail under low adhesion conditions, Tribol. Int. 75 (1) (2014) 16–23.
[8] X. Zhao, P. Zhang, Z. Wen, On the coupling of the vertical, lateral and longitudinal wheel-rail interactions at high frequencies and the resulting irregular wear, Wear 430–431 (1) (2019) 317–326.
[9] X. Zhao, Z. Li, R. Dollevoet, The vertical and the longitudinal dynamic responses of the vehicle– track system to squat type short wavelength irregularity, Veh. Syst. Dyn. 51 (12) (2013) 1918–1937.
[10] C. Chang, B. Chen, Y. Cai, J. Wang, An experimental study of high speed wheel-rail adhesion characteristics in wet condition on full scale roller rig, Wear 440–441 (1) (2019), 203092.
[11] V. Kazymyrovych, J. Bergström, F. Thuvander, Local stresses and material damping in very high cycle fatigue, Int. J. Fatig. 32 (10) (2010) 1669–1674.
[12] Y. Liu, T. Jiang, X. Zhao, Z. Wen, X. Jin, Effects of axle load transfer on wheel rolling contact fatigue of high-power AC locomotives with oblique traction rods, Int. J. Fatig. 139 (1) (2020), 105748.
[13]] J. Tunna, J. Sinclair, J. Perez, The Development of a Wheel Wear and Rolling Contact Fatigue Model, T549 Project Report, RSSB, 2007.
[14] G. Tao, X. Du, H. Zhang, et al., Development and validation of a model for predicting wheel wear in high-speed trains, J. Zhejiang Univ. - Sci. A 18 (8) (2017) 603–616.
[15] R. Deuce, Wheel Tread Damage – an Elementary Guide, Bombardier Transportation Gmbh, Netphen, Germany, 2007. Technical report.
[16] D.H. Stone, TTCI Leads Research to Cut Premature Wheel Scrapping, Railway Gazette International, 2000, pp. 593–595. September.
[17] J. Jergeus, C. Odenmarck, R. Lundenl, P. Sotkovszki, B. Karlssson, P. Gullers, Full-scale railway wheel flat experiments, P. I, Mech. Eng. F-J. Rai 213 (1) (1999) 1–13.
[18] S. Zakharov: Wheel/rail performance, in guidelines to best practices for heavy haul railway operations: wheel and rail interface issues, Int.Heavy Haul Associat.: Virginia Beach, 3–1–3-86.
[19] O. Arias-Cuevas, Z. Li, R.I. Popovici, D.J. Schipper, Simulation of curving behaviour under high traction in lubricated wheel–rail contacts, Veh. Syst. Dyn. 48 (sup1) (2010) 299–316.
[20] A. Ekberg, Fatigue of railway wheels, in: R. Lewis, U. Olofsson (Eds.), Wheel-rail Interface Handbook, Woodhead publishing, 2009, pp. 211–244.
[21] W. Zhai, X. Jin, Z. Wen, X. Zhao, Wear problems of high-speed wheel/rail systems: observations, causes, and countermeasures in China, Appl. Mech. Rev. 72 (Nov.) (2020), 060801.